applied sciences

MDPI

Article

Buckling Behavior of Non-Retrofitted and FRP-Retrofitted Steel CHS T-Joints

Amin Yazdi [1], Maria Rashidi [2], Mohammad Alembagheri [2,3,*] and Bijan Samali [2]

[1] Department of Civil and Environmental Engineering, Amirkabir University of Technology, Tehran 131565, Iran; 19626013@student.westernsydney.edu.au
[2] Centre for Infrastructure Engineering, School of Engineering, Western Sydney University, Sydney 2751, Australia; m.rashidi@westernsydney.edu.au (M.R.); b.samali@westernsydney.edu.au (B.S.)
[3] Department of Civil and Environmental Engineering, Tarbiat Modares University, Tehran 131456, Iran
* Correspondence: m.alembagheri@westernsydney.edu.au or alembagheri@modares.ac.ir; Tel./Fax: +9821-8288-4369

Abstract: This paper aims to investigate the buckling behavior of circular hollow section (CHS) T-joints in retrofitted and non-retrofitted states under axial brace compressive loading. For this purpose, two types of analysis are carried out. The first one is evaluating the critical buckling load in various tubular joints, and the other one is investigating the post-buckling behavior after each buckling mode. More than 180 CHS T-joints with various normalized geometric properties were numerically modeled in non-retrofitted state to compute their governing buckling mode, i.e., chord ovalization, brace local, or global buckling. Then three joints with different buckling modes were selected to be retrofitted by fiber-reinforced polymer (FRP) patches to illustrate the improving effect of the FRP wrapping on the post-buckling performance of the retrofitted joints. In addition, FRP composite failures were investigated. The results indicate that the FRP retrofitting is able to prevent the brace local buckling, and that matrix failure is the most common composite failure in the retrofitted joints.

Keywords: CHS T-joints; buckling mode; FRP retrofit; critical buckling load; axial compression

Citation: Yazdi, A.; Rashidi, M.; Alembagheri, M.; Samali, B. Buckling Behavior of Non-Retrofitted and FRP-Retrofitted Steel CHS T-Joints. *Appl. Sci.* **2021**, *11*, 3098. https://doi.org/10.3390/app11073098

Academic Editor: Alberto Campagnolo

Received: 6 March 2021
Accepted: 25 March 2021
Published: 31 March 2021

1. Introduction

Nowadays, the use of circular hollow sections (CHSs) in many onshore, offshore, hydraulic, and other types of structures is highly attractive. The proper performance and economic benefits of these sections in comparison with other steel sections shows their considerable potential; however, poor enforcement, design incompetence, incorrect utilization, exhaustion, accidents, or corrosion caused by environmental conditions may deteriorate the load-bearing capacity of structures made with CHSs; a critical zone is their joints. Hence, the retrofit of these structures is unavoidable in some cases. In recent years, retrofitting of steel structures with composite materials has been widely conducted, leading to a high volume of research and investigation which has resulted in improving the current retrofitting methods. There are several failure modes for the CHS, such as cracking of the welding area, plastic failure, and buckling. Under a static compressive load, one of the most important failures of CHS T-joints is the buckling of the chord or the brace in local or overall mode, such as the brace local buckling, the chord ovalization, and the brace overall buckling. In practical applications, multiple reinforcement methods can be used to increase the static (service) strength of the CHS joints, most of which can be found in literature including the use of a double plate, a collar plate, an internally stiffened ring, and local wall thickness reinforcement [1–3]. However, the mentioned methods have poor corrosion resistance; hence the use of FRP composite materials for retrofitting CHS joints has been introduced instead.

Recently, many investigations have been carried out on the effects of fiber-reinforced polymer (FRP) wrapping for steel structural joints. Chen et al. [4] investigated the static

strength of retrofitted CHS T-joints using FRP materials. They showed that the load-bearing capacity of CHS T-joints can be improved by two composite plies. This improvement was about 15% in comparison with non-retrofitted joints [4]. Lesani et al. [5] showed that the state of stresses, deformations, and ovalization of FRP-retrofitted joints are moderated in about 50% of non-retrofitted joints [5]. Haedin et al. [6] studied the effects of carbon fiber-reinforced polymer (CFRP) wrapping with concrete covering on CHS, Rectangular Hollow Section (RHS), and Square Hollow Section (SHS) joints; it has been found that the retrofitted CHS joints have better performance than SHS or RHS joints, and can therefore increase the axial stiffness of the joints [6]. Local buckling of RHS joints under axial compressive load was also investigated [7]. In a numerical evaluation, the effects of FRP wrapping on CHS T-joints under axial compressive loads were studied [8]. It revealed increasing of ultimate axial load-bearing capacity and showed that the most common composite failure mode in the chord ovalization buckling mode is compressive failure. This failure took place at 67% of the ultimate load-bearing capacity. Fam et al. [9] performed an experimental investigation on retrofitting CHS joints using both CFRP and glass fiber-reinforced polymer (GFRP) materials with the same layer conditions [9]. They showed that the load-bearing capacity increases more by the use of CFRP patches than GFRP ones, whereas Karbhari and Shully suggested the use of hybrid carbon and glass patches in order to improve durability of structures against corrosion [10]. Strengthening of thin-walled structures with FRP materials was also investigated [11]. In this research, the strength of steel hollow sections against local buckling were considered and the effects of FRP patches were evaluated.

Khodadadian et al. [12] proposed a parameter estimation framework for fracture propagation problems. The fracture problem was described by a phase-field method. Parameter estimation was realized with a Bayesian approach. They also employed the multilevel Monte Carlo finite element method to solve the stochastic Cahn–Hilliard–Cook equation [13]. In order to estimate the mild solution, they used finite elements for space discretization and the semi-implicit Euler–Maruyama method in time. Alembagheri et al. [14] numerically investigated the cyclic behavior of retrofitted and non-retrofitted CHS T-joints under axial loading. Different joints with varying ratios of brace-to-chord radius were studied. The effects of the welding process on the buckling instability of the joints in compression and the plastic failure in tension were considered. The results showed that the welding process significantly increases the plastic failure potential. Zhu et al. [15] studied the capacity of steel CHS T-joints reinforced with external stiffeners under axial compression by finite element (FE) modeling. A total of 256 T-joint FE models were established and analyzed to investigate the influence of the size of external stiffeners and joint geometry on the improvement of ultimate capacity of the joints under axial compression. Nemati et al. [16] introduced a decision-making method for selection of the most appropriate pneumatic fabric formwork for foam-filled structural panels in rapidly assembled buildings. Rashidi et al. [17,18] proposed a methodology for deriving a non-linear finite element model to analyze the behavior of high strength concrete columns wrapped with CFRP jackets and reinforced with axial and helical steel bars. Additional research related to the application of strengthening methods to other types of structures is available [19–21].

The purpose of this research is to investigate the performance of CHS T-joints strengthened by the FRP patches as an external coverage under monotonic compressive loading. The study consists of evaluating the governing buckling mode of CHS T-joints, the effects of FRP wrapping on the ultimate load capacity, and evaluation of the post-buckling behavior. The adopted methodology is numerical modeling of the joints with the finite element method, and the results will be presented in terms of various buckling modes.

2. CHS T-Joints

A schematic representation of a non-retrofitted CHS T-joint including a chord member, a brace member, and their geometric features are shown in Figure 1. Based on the literature, the most important normalized geometric properties of non-retrofitted joints, which are studied in this research, are the ratio of the brace radius to its thickness (r/t), the ratio of

the chord radius to its thickness (R/T), the ratio of the brace to the chord radius (r/R), and the ratio of the brace length to its radius (l/r). Independent varying of the geometric parameters will lead to a huge number of models; hence, in this study the radii of the members are considered as constant: r = 70 mm and R = 80 mm. Therefore, the r/R ratio is constant but the remaining normalized parameters are independently varied over reasonable ranges in order to investigate their effects on the buckling response of the generated CHS T-joints. The selected parameters and ranges are tabulated in Table 1. Accordingly, more than 180 non-retrofitted CHS T-joints are modeled to find out the effects of the geometric parameters on the governing buckling modes and their critical loads.

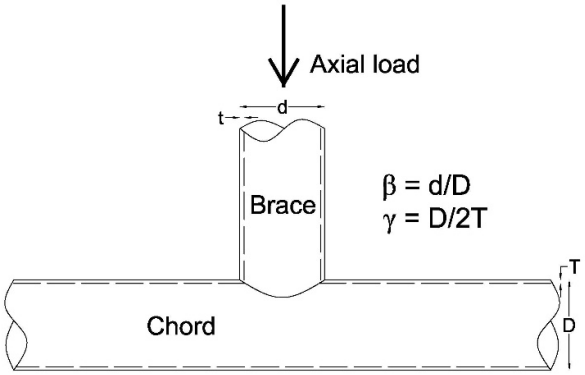

Figure 1. Geometric features of a typical circular hollow section (CHS) T-joint without retrofit. $D = 2R$; $d = 2r$.

Table 1. The geometric properties of the tubular CHS T-joints and their varying range in this study.

Geometric Property	Varying Range
r/t	8–65
R/T	8–24
l/r	5–17

After investigation of the non-retrofitted joints, three joints with different buckling behavior (i.e., the local and overall buckling of the brace and the chord ovalization) were chosen to be retrofitted. When the joints were retrofitted with FRP wrapping, additional parameters were added to the problem. These were the number of plies in the composite patches (2–12 plies in this study), the ply orientation, and the length of the composite patch, which was changed from half to the total brace length. In practice, the CFRP wrapping method is directly disarrayed because of the T-shape of the joint; hence, in this numerical study, just practical wrappings are considered. The buckling state of the retrofitted joints and their post-buckling behavior were assessed and then compared with the corresponding non-retrofitted joints. In this way, the effects of the FRP wrapping on the load-bearing capacity and the deformed shape of the joints were investigated. Composite failures in the retrofitted joints were also evaluated.

2.1. Numerical Modeling

The joints were made from steel with elastic-perfectly plastic behavior assuming Young's Modulus of 219 GPa, Poisson's ratio of 0.3, the density of 7800 kg/m^3, and the Yielding stress of 383 MPa. The steel material obeys the von Mises yield criterion and the associated flow rule as the classical plasticity model. For retrofitting of the selected CHS joints, the carbon fiber-reinforced polymer (CFRP) material was utilized due to its popularity with the thickness of 0.125 mm; the properties of the composite material are presented in Table 2. In this table, subscripts 1 and 2 show the fiber longitudinal and transversal directions, respectively. The Hashin damage criteria [22,23] are used to consider the FRP failure with the properties listed in Table 2.

Table 2. Properties of the carbon fiber-reinforced polymer (CFRP) composite material used in this study.

Material	Properties	
	Stress Analysis	**Failure Analysis (MPa)**
Carbon/epoxy	E_1 = 23,000 MPa $E_2 = E_3$ = 14,816 MPa $\nu_{12} = \nu_{13} = \nu_{23}$ = 0.25 $G_{12} = G_{13}$ = 7408 MPa G_{23} = 2963 MPa	X_T = 1062 X_c = 610 Y_T = 31 Y_c = 118 $S_{12} = S_{13}$ = 72 S_{23} = 20

The joints were modeled using the finite element method with the ABAQUS software package. Two types of analysis were carried out. First, the linear perturbation analysis was adopted in order to investigate the geometric effects on the buckling modes and the critical loads of the selected CHS T-joints. In this analysis, the loading scenario was a static monotonic compressive loading along the brace as shown in Figure 1. Then the post-buckling analysis was done to evaluate the post-buckling behavior in different buckling modes. In this step, the loading scenario is displacement-based as a static monotonic compressive displacement along the brace. The displacement-based approach was selected because the post-buckling behavior and ductility can be entirely evaluated. The governing equations were displacement-based equations with regards to the static analysis. In these equations, the stiffness and mass matrices as well as the loading vector was constructed based on the discretized finite element mesh. For the purpose of retrofitting, three joints with different governing buckling modes were considered. Their properties will be represented in the next sections.

The CHS joints were three-dimensionally modeled with brick elements while the FRP patches were modeled using 3D shell elements, which were fully bonded to the steel surface. The used solid and shell elements were first-order with linear shape functions. The brace's end was constrained in the plane of its cross-section, but no constraint was applied along its length for possibility of applying static compressive load. All rotational degrees of freedom at the brace end were also constrained. Both ends of the chord were pinned, hence the transitional degrees of freedom along with the rotational degree of freedom about the longitudinal chord axis were constrained.

2.2. Verification Study

The numerical procedure was verified using various CHS T-joints in retrofitted and non-retrofitted states. Due to the matter of brevity, the results of a typical CHS T-joint are presented, having been previously studied by Lesani et al. [5] both numerically and experimentally. Its geometrical properties are represented in Table 3. The mesh objectivity study was done to reach a reasonable mesh density that results in accurate results. The resulted axial load-displacement curve (at the brace end) is shown in Figure 2 and compared with the work by Lesani et al. [5]. The obtained curve is in good agreement with the previous experimental and numerical results.

Table 3. Geometric properties of the CHS T-joint for the verification study [5,8].

Chord Thickness, T (mm)	Brace Thickness, t (mm)	Chord Length, L (mm)	Brace Length, l (mm)	Chord Radius, R (mm)	Brace Radius, r (mm)	F_y (MPa)
6.35	8.56	1845	570	136.5	57.2	385

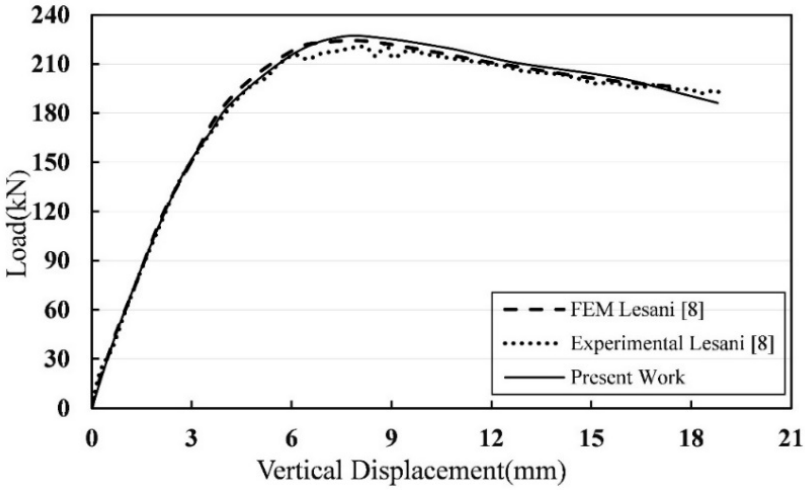

Figure 2. Load-displacement curve of the verified CHS T-joint under axial brace compressive load.

3. Results and Discussion

At first, the effects of the geometric properties on the critical buckling load and the governing buckling mode of the non-retrofitted CHS T-joints were studied by modeling more than 180 joints, as explained in the previous section. Then, three joints with different buckling modes were retrofitted to investigate the effects of FRP retrofitting on the buckling behavior of the CHS T-joints. The failure modes predicted are in agreement with the previous experimental results [5,7,8].

3.1. Non-Retrofitted Joints

The obtained results show that there are three main buckling modes. They are the local and overall buckling of the brace and the chord ovalization. These buckling modes are illustrated in Figure 3. The common elephant-foot buckling is observed in the brace local buckling. The brace overall buckling happens out of the plane of the joint because the high flexural stiffness of the chord prevents in-plane buckling.

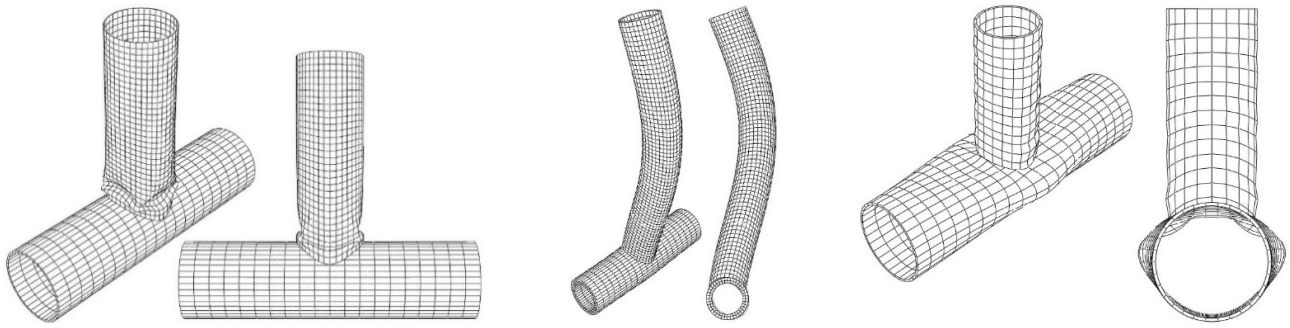

(**a**) (**b**) (**c**)

Figure 3. The main buckling modes of the CHS T-joints: (**a**) the brace local buckling; (**b**) the brace overall buckling; and (**c**) the chord ovalization.

Figure 4 shows the distribution of the buckling modes of the non-retrofitted CHS T-joints along with their critical buckling load in terms of the most important normalized geometric properties. The most buckling occurs in brace local buckling. Generally, the chord ovalization buckling mode has the lowest critical load. As it is observed in Figure 4a, for the joints with $r/t < 10$ the critical modes are the brace overall buckling or the chord ovalization, with the brace overall buckling showing more buckling load. By increasing

the r/t ratio, the brace local buckling is observed such that for the joints with $r/t > 30$ the brace local buckling is the most critical mode.

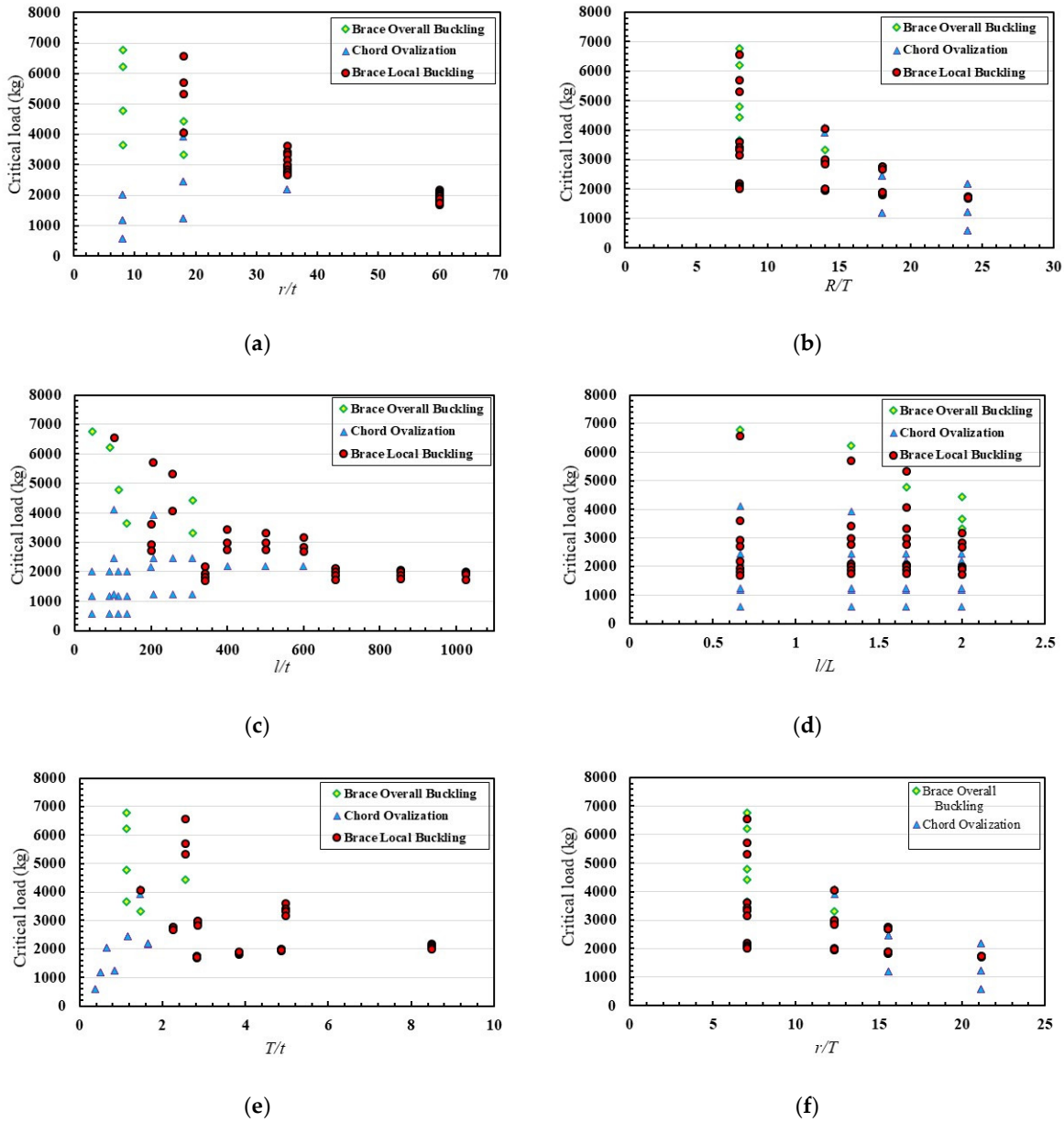

Figure 4. Distribution of the buckling modes and their critical buckling load (kg) in terms of dimensionless values: (**a**) the brace's r/t; (**b**) the chord's R/T; (**c**) the brace's l/t; (**d**) the ratio of the brace to the chord length l/L; (**e**) the ratio of the chord to the brace thickness T/t; and (**f**) the brace's r/T.

From Figure 4b, for the ratio of the chord's R/T, if this ratio is less than 10, no chord ovalization occurs. For a ratio higher than 15, no brace overall buckling is observed. The brace's l/t ratio in Figure 4c can separate the brace local buckling from the other buckling modes for values more than 600 or less than 100. The brace to the chord length ratio l/L shows no clear sign of separation between the buckling modes or their critical load (Figure 4d). For the chord to the brace thickness ratio T/t in Figure 4e, values of more than 3 will lead to the brace local buckling. However, values less than 1.5 will lead to the two other buckling modes. The brace's l/r ratio (Figure 4f) cannot clearly divide the buckling modes.

3.2. Retrofitted Joints

From the non-retrofitted joints, three joints with different governing buckling modes were selected for retrofitting. The properties of these joints and their critical buckling modes are listed in Table 4. The joints were retrofitted with FRP patches in various orientation, length, and number of plies to investigate their effects on the buckling and post-buckling response.

Table 4. The properties of the selected CHS T-joints for retrofitting.

Joint Name	*l* (mm)	*L* (mm)	*d* (mm)	*D* (mm)	*t* (mm)	*T* (mm)	Buckling Mode
T1	400	600	121	159	4.5	4.5	Chord ovalization
T2	1000	600	140	159	9	15	Brace overall buckling
T3	400	600	140	159	2.5	10	Brace local buckling

3.2.1. Joint T1 (Chord Ovalization)

The chord ovalization happens by local deformation of the chord in the interface of the chord and the brace under brace compressive load. The before- and post-buckling axial load-displacement curve of the T1 joint in the non-retrofitted state considering large deformation is shown in Figure 5. The joint behaves linearly until the buckling point where the negative slope occurs. This is the main buckling part that is studied here. By increasing the displacement, a hardening section is started until the ultimate load bearing capacity of the joint is reached; after that, it undergoes softening until the failure.

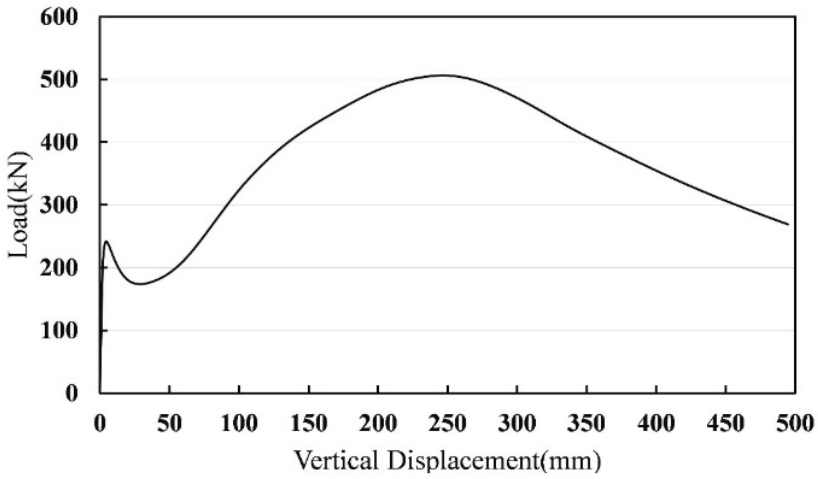

Figure 5. The axial load-displacement curve of the T1 joint (the chord ovalization buckling mode) considering large deformation.

In order to increase the critical load in the chord ovalization buckling mode, the FRP patches were wrapped just around the chord of the T1 joint, utilizing various numbers of plies and layer distributions. The obtained axial load-deformation curves are compared in Figure 6. In Figure 6a, the 4-layer FRP wrapping increases the critical buckling load of the joint. The best performance belongs to the ply distributions of (0/90)s and (0/0)s. In the 0° orientation, the fiber directions are in the chord circumferential direction, while for the 90° orientation, the fibers are in the chord longitudinal axis direction. In this way, the FRP wrapping moderates the ovalizing and flexural deformation of the chord. The lowest increase belongs to the (90/90)s distribution in which all fibers are oriented along the chord axis.

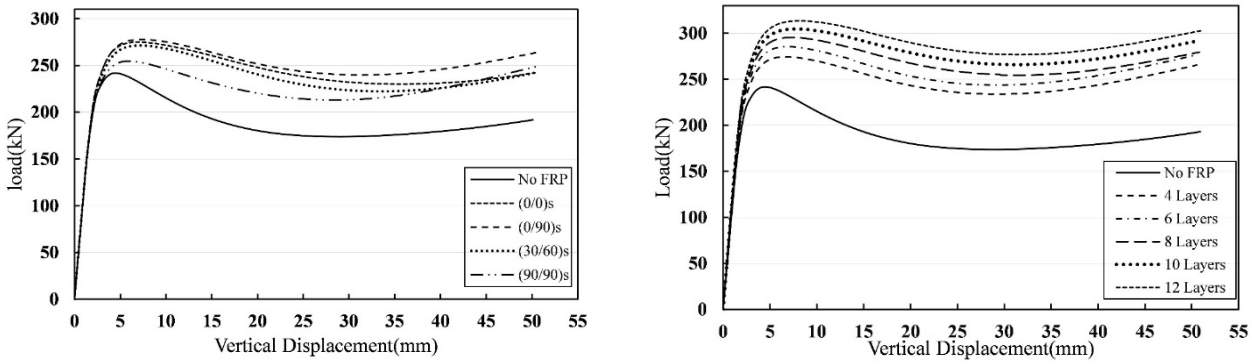

(**a**) (**b**)

Figure 6. The effect of (**a**) ply distributions, and (**b**) number of plies, on the axial load-displacement curve of the retrofitted T1 joint.

The effect of the number of plies was investigated by the use of 4, 8, 10, and 12 plies with (0/90)s distribution. The same buckling mode was observed for the retrofitted joint; the critical buckling load increased about 14% for 4 plies, and up to 30% for 12 plies. More layers cause additional increase in the critical buckling load.

The critical composite failure of the FRP patches controlling the chord ovalization buckling mode is the matrix tension as shown in Figure 7. Under this buckling mode, the failure of composite initiates and propagates around the hoop line on both sides of the chord. These regions are critical for the fiber tension failure as well.

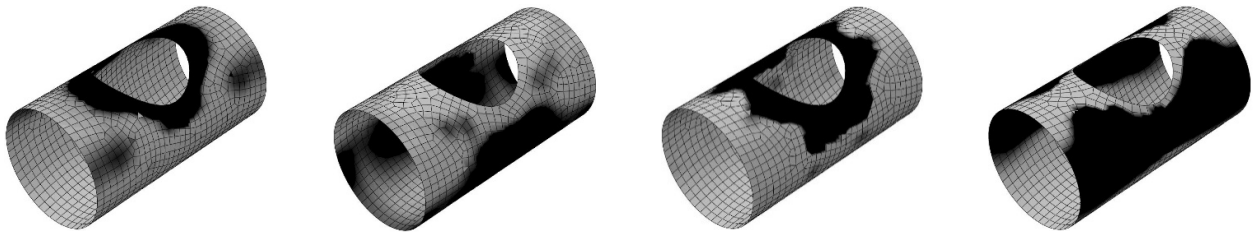

(**a**) (**b**) (**c**) (**d**)

Figure 7. Failure of the fiber-reinforced polymer (FRP) patches in the retrofitted T1 joint (the chord ovalization buckling mode). Composite failure modes: (**a**) fiber compression; (**b**) fiber tension; (**c**) matrix compression; (**d**) matrix tension.

3.2.2. Joint T2 (Brace Overall Buckling)

The axial load-displacement curve of the non-retrofitted T2 joint assuming large deformation is shown in Figure 8. The critical buckling load of the non-retrofitted T2 joint is about 120 kN, and the buckling happens out of the plane of the joint as shown in Figure 3b. The joint behaves linearly until the buckling point where the softening initiates and continues to the failure. Unlike the chord ovalization mode, no hardening section is observed in the post-buckling behavior under this mode of buckling.

In order to improve the buckling behavior, various brace-retrofitted length and ply distributions of FRP wrapping were modeled. In all of the retrofitted cases, four plies with the distribution of (0/90)s were applied to the chord. The obtained axial load-displacement curves are compared in Figure 9. When the brace was retrofitted with 8 plies with various orientations (Figure 9a), the retrofitting hardly increased the critical load; it caused just about 8% improvement for (90/90)2s distribution. It means that the fibers should be in the direction of the brace longitudinal axis. This low increase is because increasing the moment of inertia by FRP wrapping is insignificant. The same buckling mode was observed for the retrofitted joint.

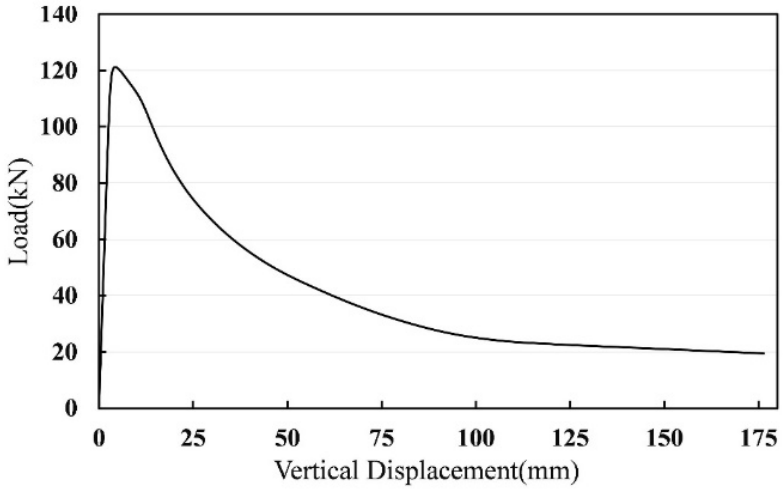

Figure 8. The axial load-displacement curve of the T2 joint (the brace overall buckling mode).

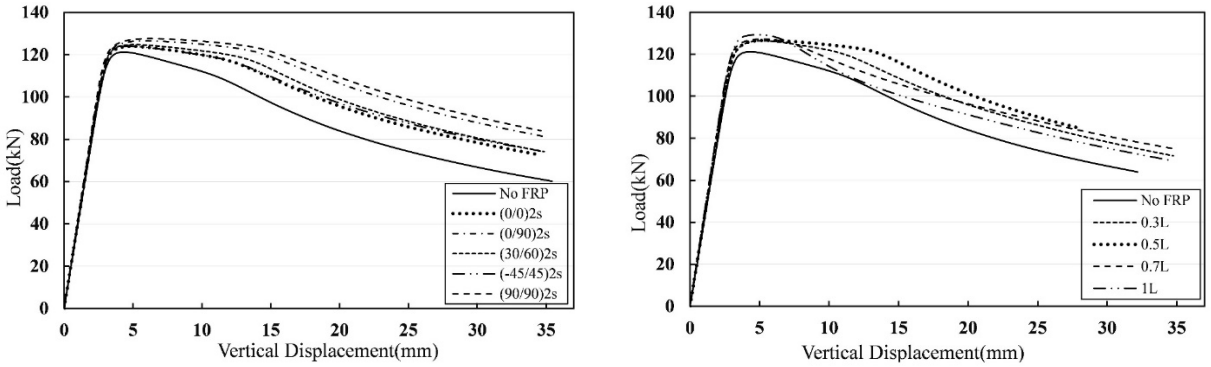

(**a**) (**b**)

Figure 9. The effect of (**a**) ply distributions, and (**b**) retrofitted brace length, on the axial load-displacement curve of the retrofitted T2 joint.

Investigation of the brace retrofitted length with 8 plies of (90/90)2s distribution shows that the use of FRP composite with the length of equal or less than half of the brace length may improve the post-buckling behavior by decreasing the effective buckling length. Longer lengths may partly increase the critical load by increasing the moment of inertia. In general, the FRP retrofitting cannot significantly improve the post-buckling behavior of the CHS T-joints, if the governing buckling mode is the brace overall buckling.

The composite FPR failure under the brace overall buckling is shown in Figure 10. In this buckling mode, the matrix tension and compression failures are the most possible FRP failure because of the inherent weakness of the matrix behavior, especially under tension loads. Initiation of the matrix tension failure happens in 40% of the buckling load. This failure initiates at the Crown Point, and by increasing the displacement, this failure zone may propagate to upper parts of the brace composite patch.

3.2.3. Joint T3 (Brace Local Buckling)

The axial load-displacement curve of the non-retrofitted T3 joint is shown in Figure 11. The buckling happens when the vertical displacement of the brace end reaches to about 2 mm, where the first wrinkle is observed near the chord–brace intersection. This local buckling leads to a sudden significant reduction of about 72% in the load-bearing capacity. By increasing the brace end displacement, successive minor hardenings appear, which are stopped by successive wrinkles above the first local buckling. This process causes a

vibration shape in the load-displacement curve shown in Figure 11. The final deformed shape of the local buckling, including the successive wrinkles, is depicted in Figure 12.

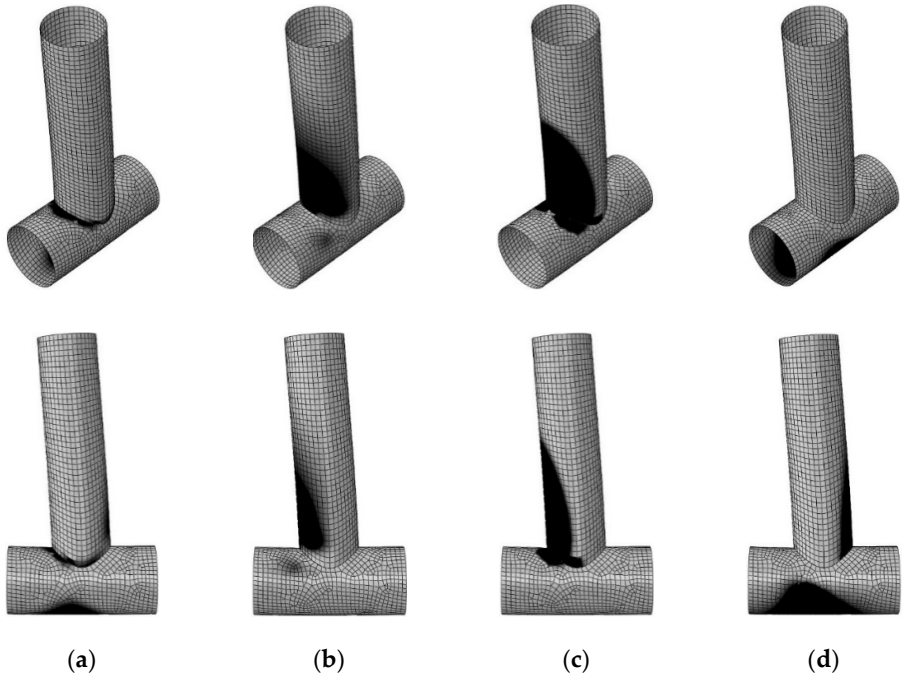

Figure 10. Failure of the FRP patches in the retrofitted T2 joint (the brace overall buckling mode). Composite failure modes: (**a**) fiber compression; (**b**) fiber tension; (**c**) matrix compression; (**d**) matrix tension.

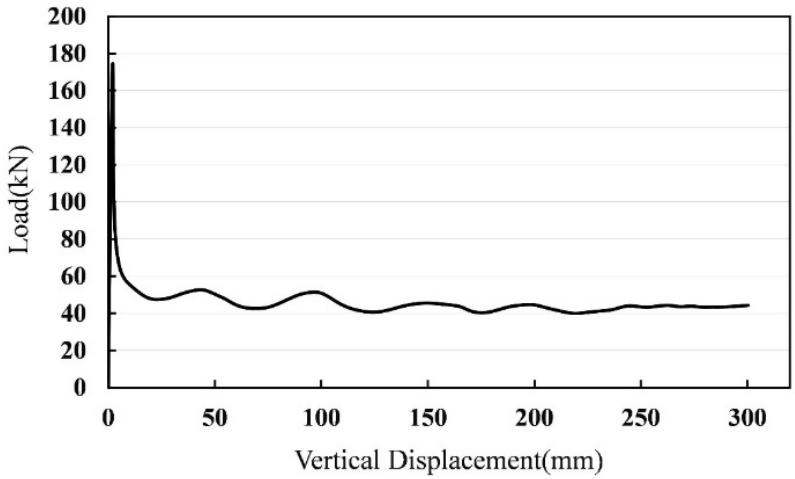

Figure 11. The axial load-displacement curve of the T3 joint (the brace local buckling mode).

In order to improve or prevent the brace local buckling, the FRP patches were wrapped just around the brace member. In the first step, various ply distributions were considered to show their effects; for this purpose, two plies were used in all cases. As represented in Figure 13a,b, just two plies of FRP can prevent the sudden decrease of the load bearing due to the local brace buckling and change the governing buckling mode to the chord ovalization. If the fibers are oriented in the brace longitudinal axis, i.e., (90/90) distribution, the FRP patches start to carry the load by applying the axial load, hence the FRP failure happens faster than when the fibers are oriented in the brace circumferential distribution. Hence, the (90/90) distribution leads to the higher ultimate load while the (0/0) distribution shows higher durability. From Figure 14b, the retrofit of the brace with more number of

FRP plies but with the same distribution has little effect on the post-buckling behavior of the joint.

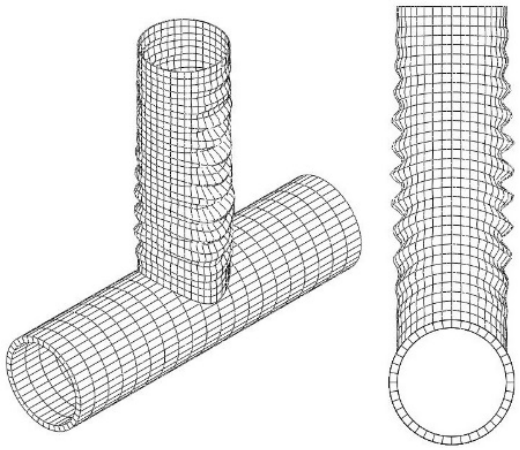

Figure 12. A typical wrinkle on the brace wall.

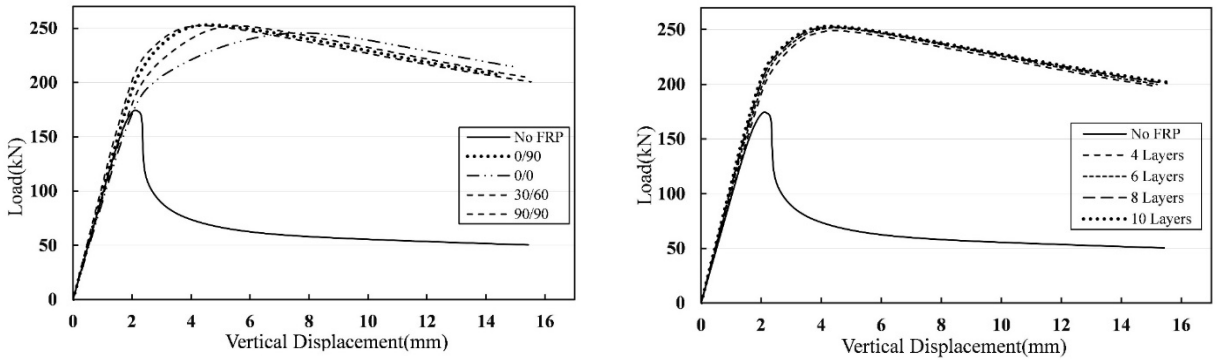

(**a**) (**b**)

Figure 13. The effect of (**a**) ply distributions, and (**b**) number of plies, on the axial load-displacement curve of the retrofitted T3 joint.

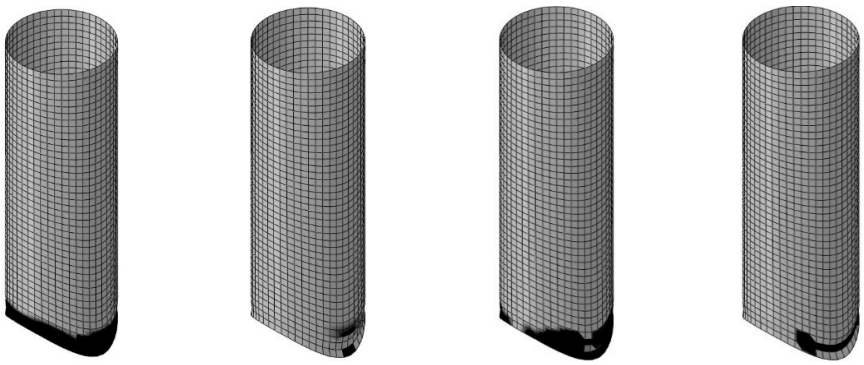

(**a**) (**b**) (**c**) (**d**)

Figure 14. Failure of the FRP patches in the retrofitted T3 joint (the brace local buckling mode). Composite failure modes: (**a**) fiber compression; (**b**) fiber tension; (**c**) matrix compression; (**d**) matrix tension.

The possible composite failures are shown in Figure 14. The critical zone for the composite failures is near the intersection of the brace and the chord. It is revealed that the fiber and matrix compression modes are more critical than the other modes.

4. Conclusions

The buckling and post-buckling behavior of the CHS T-joints under monotonic compressive loading was evaluated using more than 180 joints with various geometric properties. The joints were numerically modeled utilizing the finite element method. The brace local buckling is the most common buckling mode of the CHS T-joints in the considered range of parameters and results in a sudden significant reduction in the load carrying of the joint. Investigation of the geometric properties of the non-retrofitted CHS T-joint showed that mode in which buckling occurs most often is the brace local buckling. Generally, the chord ovalization buckling mode has the lowest critical load. For the joints with $r/t < 10$, the critical modes are the brace overall buckling or the chord ovalization, with the brace overall buckling showing more buckling load. By increasing the r/t ratio, the brace local buckling is observed such that for the joints with $r/t > 30$, the brace local buckling is the most critical mode. For the ratio of the chord's R/T, if this ratio is less than 10, no chord ovalization occurs. But for a ratio of more than 15, no brace overall buckling is observed. The brace's l/t ratio can separate the brace local buckling from the other buckling modes for values over than 600 or less than 100. The brace to the chord length ratio l/L shows no clear sign of separation between the buckling modes or their critical load. But for the chord to the brace thickness ratio T/t, values greater than 3 will lead to the brace local buckling. However, the values less than 1.5 will lead to the two other buckling modes. The brace's l/r ratio cannot clearly divide the buckling modes.

The retrofit of CHS T-joints by the use of FRP composite patches may improve their load-bearing capacity. The results show good performance of the composite patches which can be concluded as follows:

1. In the chord ovalization buckling mode, the use of FRP wrapping may improve the load bearing capacity of the retrofitted joints up to 40% in comparison with non-retrofitted ones.
2. Effectiveness of the FRP wrapping in the chord ovalization buckling mode is considerable when at least four plies with the distribution of (0/0)s and (0/90)s are utilized.
3. Investigation of the FRP wrapping performance in various buckling modes shows that this method may totally prevent the brace local buckling and modify destructive effects of the chord ovalization. This method has poor performance in the brace overall buckling.
4. The matrix tension failure is the most common composite failure in the chord ovalization and the brace overall buckling, but the matrix compressive failure is most possible in the brace local buckling.
5. The FRP wrapping can improve the load bearing capacity of the CHS T-joints; this method can increase the ultimate load-bearing capacity about 17% and 50% respectively in the overall and local brace buckling.

Author Contributions: Formal analysis, A.Y.; Funding acquisition, M.R.; Investigation, A.Y. and M.A.; Methodology, M.A.; Project administration, B.S.; Resources, M.R.; Software, A.Y.; Supervision, B.S.; Validation, M.A.; Visualization, B.S.; Writing—original draft, M.A.; Writing—review & editing, M.R. All authors have read and agreed to the published version of the manuscript.

Funding: This research received no external funding.

Conflicts of Interest: The authors declare no conflict of interest.

References

1. Choo, Y.; Van der Vegte, G.; Zettlemoyer, N.; Li, B.; Liew, J. Static strength of T-joints reinforced with doubler or collar plates. I: Experimental investigations. *J. Struct. Eng.* **2005**, *131*, 119–128.
2. Gandhi, P.; Raghava, G.; Murthy, D.R. Fatigue behavior of internally ring-stiffened welded steel tubular joints. *J. Struct. Eng.* **2000**, *126*, 809–815. [CrossRef]
3. Li, T.; Shao, Y. Study on hysteretic behavior of square tubular T-joints with increased chord thickness. *Jianzhu Jiegou Xuebao (J. Build. Struct.)* **2011**, *32*, 142–150.
4. Chen, C.; Shao, Y.B.; Yang, J. Study on Static Strength of Circular Hollow Section (CHS) T-Joint Reinforced with FRP. *Appl. Mech. Mater.* **2011**, *99*, 72–75. [CrossRef]
5. Lesani, M.; Bahaari, M.; Shokrieh, M. Experimental investigation of FRP-strengthened tubular T-joints under axial compressive loads. *Constr. Build. Mater.* **2014**, *53*, 243–252. [CrossRef]
6. Haedir, J.; Bambach, M.R.; Zhao, X.L.; Grzebieta, R.H. Strength of circular hollow sections (CHS) tubular beams externally reinforced by carbon FRP sheets in pure bending. *Thin-Walled Struct.* **2009**, *47*, 1136–1147. [CrossRef]
7. Aguilera, J.; Fam, A. Retrofitting tubular steel T-joints subjected to axial compression in chord and brace members using bonded FRP plates or through-wall steel bolts. *Eng. Struct.* **2013**, *48*, 602–610. [CrossRef]
8. Lesani, M.; Bahaari, M.; Shokrieh, M. Numerical investigation of FRP-strengthened tubular T-joints under axial compressive loads. *Compos. Struct.* **2013**, *100*, 71–78. [CrossRef]
9. Fam, A.; Witt, S.; Rizkalla, S. Repair of damaged aluminum truss joints of highway overhead sign structures using FRP. *Constr. Build. Mater.* **2006**, *20*, 948–956. [CrossRef]
10. Karbhari, V.; Shulley, S. Use of composites for rehabilitation of steel structures-determination of bond durability. *J. Mater. Civ. Eng.* **1995**, *7*, 239–245. [CrossRef]
11. Shamsuddoha, M.; Islam, M.M.; Aravinthan, T.; Manalo, A.; Lau, K.T. Effectiveness of using fibre-reinforced polymer composites for underwater steel pipeline repairs. *Compos. Struct.* **2013**, *100*, 40–54. [CrossRef]
12. Khodadadian, A.; Noii, N.; Parvizi, M.; Abbaszadeh, M.; Wick, T.; Heitzinger, C. A Bayesian estimation method for variational phase-field fracture problems. *Comput. Mech.* **2020**, *66*, 827–849. [CrossRef] [PubMed]
13. Khodadadian, A.; Parvizi, M.; Abbaszadeh, M.; Dehghan, M.; Heitzinger, C. A multilevel Monte Carlo finite element method for the stochastic Cahn–Hilliard–Cook equation. *Comput. Mech.* **2019**, *64*, 937–949. [CrossRef] [PubMed]
14. Alembagheri, M.; Rashidi, M.; Yazdi, A.; Samali, B. Numerical Analysis of Axial Cyclic Behavior of FRP Retrofitted CHS Joints. *Materials* **2021**, *14*, 648. [CrossRef]
15. Zhu, L.; Song, Q.; Bai, Y.; Wei, Y.; Ma, L. Capacity of steel CHS T-Joints strengthened with external stiffeners under axial compression. *Thin-Walled Struct.* **2017**, *113*, 39–46. [CrossRef]
16. Nemati, S.; Rashidi, M.; Samali, B. Decision making on the optimised choice of pneumatic formwork textile for foam-filled structural composite panels. *Int. J. GEOMATE* **2017**, *13*, 220–228. [CrossRef]
17. Rashidi, M. Finite element modeling of FRP wrapped high strength concrete reinforced with axial and helical reinforcement. *Int. J. Emerg. Technol. Adv. Eng.* **2014**, 728–735.
18. Rashidi, M.; Ghodrat, M.; Samali, B.; Kendall, B.; Zhang, C. Remedial modelling of steel bridges through application of analytical hierarchy process (AHP). *Appl. Sci.* **2017**, *7*, 168. [CrossRef]
19. Ganji, H.T.; Alembagheri, M.; Khaneghahi, M.H. Evaluation of seismic reliability of gravity dam-reservoir-inhomogeneous foundation coupled system. *Front. Struct. Civ. Eng.* **2019**, *13*, 701–715. [CrossRef]
20. Alembagheri, M.; Estekanchi, H.E. Nonlinear analysis of aboveground anchored steel tanks using endurance time method. *Asian J. Civ. Eng.* **2011**, *12*, 731–750.
21. Yazdani, Y.; Alembagheri, M. Effects of base and lift joints on the dynamic response of concrete gravity dams to pulse-like excitations. *J. Earthq. Eng.* **2017**, *21*, 840–860. [CrossRef]
22. Hashin, Z.; Rotem, A. A fatigue failure criterion for fiber reinforced materials. *J. Compos. Mater.* **1973**, *7*, 448–464. [CrossRef]
23. Hashin, Z. Failure criteria for unidirectional fiber composites. *J. Appl. Mech.* **1980**, *47*, 329–334. [CrossRef]